On the causes of pressure oscillations in low-permeable and low-compressible porous media

Joachim Berdal Haga[1,2,*], Harald Osnes[1,2] and Hans Petter Langtangen[1,3]

[1] *Scientific Computing Department, Simula Research Laboratory, Norway*
[2] *Department of Mathematics, University of Oslo, Norway*
[3] *Department of Informatics, University of Oslo, Norway*

SUMMARY

Non-physical pressure oscillations are observed in finite element calculations of Biot's poroelastic equations in low-permeable media. These pressure oscillations may be understood as a failure of compatibility between the finite element spaces, rather than elastic locking. We present evidence to support this view by comparing and contrasting the pressure oscillations in low-permeable porous media with those in low-compressible porous media. As a consequence, it is possible to use established families of stable mixed elements as candidates for choosing finite element spaces for Biot's equations. Copyright © 2000 John Wiley & Sons, Ltd.

KEY WORDS: Biot's consolidation; pressure oscillations; elastic locking; low-permeable media; finite elements

1. Introduction

The coupled poroelastic equations due to Biot [1] describe the behaviour of fluid-filled porous materials undergoing deformation. It is well known that the finite element solution of these equations may exhibit unphysical oscillations in the fluid pressure under certain conditions — low permeabilities, early times (shocks), and short time steps [2, 3, 4]. For the practitioner it is important to know why non-physical oscillations may occur and how to avoid them. This is the research problem we address in the present paper.

Several methods have been proposed to remove the spurious pressure oscillations. Murad *et al.* [4, 5] considered the displacement/fluid pressure (two-field) form of Biot's equation, and identified the initial state (early times) consolidation problem as an instance of the Stokes saddle-point problem, with an associated inf-sup stability test. They developed short- and long-term error bounds for some continuous pressure elements. In particular, they found that the oscillations decay in time and may be treated by post-processing even with unstable element combinations. Wan [6] employed a stabilised finite element

---

method, based on the Galerkin least-squares method, on the two-field and the displacement/fluid velocity/fluid pressure (three-field) formulations. Wan pointed out that the oscillations do not decay, and may even be amplified, under different assumptions, in particular in heterogeneous materials with low-permeable layers. Another stabilisation method was proposed by Aguilar *et al.* [7], who employ a perturbation term depending only on *a priori* material and grid parameters.

More recently, least-squares mixed finite element methods for the stress tensor/displacement/fluid velocity/fluid pressure four-field formulation have been proposed by Korsawe and Starke [8] and Tchonkova *et al.* [9]. These methods have elliptic variational representations and hence appear to be naturally stable.

Phillips and Wheeler [10] investigated the same three-field variant of Biot's equation as Wan, and identified the oscillation phenomenon for short time steps and early times as related to (in-)elastic locking, observed in linear elasticity [11]: The reduction of effective degrees of freedom (owing to vanishing divergence) "locks" the displacement solution.

In the present paper, we investigate the characteristics of the poroelastic fluid pressure oscillations and compare them to those of elastic locking and inf-sup violation. The similarity with the solid pressure oscillations in elasticity is investigated, in part through a mathematical analogy with the elasticity problem and in part through extending the two- and three-field poroelastic formulations to mixed formulations which includes the solid pressure. The addition of a solid pressure field is known to overcome the locking problem in pure elasticity.

Our idea is to link the fluid pressure oscillations to a violation of the compatibility requirements for the discrete finite element spaces. Careful investigations performed in the paper support the view that these phenomena are related. We can then draw upon a large body of knowledge regarding stable spaces for saddle-point problems. This approach helps us to formulate hypotheses about stable mixed finite elements for two-, three-, and four-field formulations of poroelasticity. We test the validity of the hypotheses through extensive numerical experiments. The results form a body of evidence for our goal of giving practitioners a range of choices for the robust solution of Biot's equations, whether the requirement is a fast solver (which might use a two-field formulation with the minimal-order stable elements) or higher-order accuracy.

2. The mathematical model

The equations describing poroelastic flow and deformation are derived from the principles of conservation of fluid mass and the balance of forces on the porous matrix. The linear poroelastic equations can, in the small-strains regime, be expressed as

$$S\dot{p}_{\mathrm{f}} - \boldsymbol{\nabla} \cdot \boldsymbol{\Lambda}\boldsymbol{\nabla}p_{\mathrm{f}} + \alpha\boldsymbol{\nabla} \cdot \dot{\boldsymbol{u}} = q, \tag{1}$$

$$\boldsymbol{\nabla}(\lambda + \mu)\boldsymbol{\nabla} \cdot \boldsymbol{u} + \boldsymbol{\nabla} \cdot \mu\boldsymbol{\nabla}\boldsymbol{u} - \alpha\boldsymbol{\nabla}p_{\mathrm{f}} = \boldsymbol{r}. \tag{2}$$

Here, $\boldsymbol{r}$ represents the total body forces, and q is a fluid injection rate. The primary variables are p_{f} for the fluid pressure and $\boldsymbol{u}$ for the displacement of the porous medium. Furthermore, S and $\boldsymbol{\Lambda}$ are the fluid storage coefficient and the flow mobility respectively, α is the Biot-Willis fluid/solid coupling coefficient, and λ and μ are the Lamé elastic parameters.

The fluid (Darcy) velocity is often of particular interest in poroelastic calculations. It can be written

$$\boldsymbol{v}_{\mathrm{D}} = -\boldsymbol{\Lambda}(\boldsymbol{\nabla}p_{\mathrm{f}} - \boldsymbol{r}_{\mathrm{f}}), \tag{3}$$

and represents the net macroscopic flux, given body forces $\boldsymbol{r}_\mathrm{f}$ acting on the fluid phase. For the displacement equation, the main secondary quantity of interest is the effective stress tensor,

$$\sigma' = \sigma - \alpha p_\mathrm{f}\mathbf{I} = (\lambda\operatorname{Tr}\varepsilon - \alpha p_\mathrm{f})\mathbf{I} + 2\mu\varepsilon, \tag{4}$$

which is written in terms of the small-strains tensor

$$\varepsilon = (\boldsymbol{\nabla}\boldsymbol{u} + \boldsymbol{\nabla}\boldsymbol{u}^\mathsf{T})/2. \tag{5}$$

In the following, this canonical form of Biot's equation given in Equations (1)–(2) is referred to as the two-field formulation.

Weak discrete-in-time form. We employ a first-order backward finite difference method in time, which leads to the discrete-time form of Equation (1)

$$S p_\mathrm{f} - \Delta t\boldsymbol{\nabla}\cdot\boldsymbol{\Lambda}\boldsymbol{\nabla}p_\mathrm{f} + \alpha\boldsymbol{\nabla}\cdot\boldsymbol{u} = q\Delta t + S\hat{p}_\mathrm{f} + \alpha\boldsymbol{\nabla}\cdot\hat{\boldsymbol{u}}. \tag{6}$$

Hatted variables $(\hat{p}_\mathrm{f}, \hat{\boldsymbol{u}})$ indicate values from the previous time step, while unmarked variables are taken to be at the current time step.

Next, we rewrite Equation (2) and (6) in weak form, using integration by parts to eliminate second derivatives. We define the following (bi-)linear forms on the domain Ω with boundary Γ,

$$\begin{aligned}
a_\mathrm{f}^\mathrm{I}(\phi_\mathrm{f}, p_\mathrm{f}) &= -\int_\Omega S\phi_\mathrm{f}p_\mathrm{f} + \Delta t\boldsymbol{\nabla}\phi_\mathrm{f}\cdot\boldsymbol{\Lambda}\boldsymbol{\nabla}p_\mathrm{f}\,\mathrm{d}\Omega, \\
b^\mathrm{I}(\phi_\mathrm{f}, \boldsymbol{u}) &= -\int_\Omega \alpha\phi_\mathrm{f}\boldsymbol{\nabla}\cdot\boldsymbol{u}\,\mathrm{d}\Omega, \\
l_\mathrm{f}^\mathrm{I}(\phi_\mathrm{f}) &= -\int_\Omega(q\Delta t + S\hat{p}_\mathrm{f} + \boldsymbol{\nabla}\cdot\hat{\boldsymbol{u}})\phi_\mathrm{f}\,\mathrm{d}\Omega + \int_\Gamma \phi_\mathrm{f}(f_{\boldsymbol{n}} - \boldsymbol{n}\cdot\boldsymbol{\Lambda}\boldsymbol{r}_\mathrm{f})\Delta t\,\mathrm{d}\Gamma,
\end{aligned} \tag{7}$$

and

$$\begin{aligned}
a_\mathrm{u}^\mathrm{I}(\boldsymbol{\phi}_\mathrm{u}, \boldsymbol{u}) &= \int_\Omega[\lambda(\boldsymbol{\nabla}\cdot\boldsymbol{\phi}_\mathrm{u})(\boldsymbol{\nabla}\cdot\boldsymbol{u}) + \mu\boldsymbol{\nabla}\boldsymbol{\phi}_\mathrm{u}:\boldsymbol{\nabla}\boldsymbol{u}]\,\mathrm{d}\Omega, \\
l_\mathrm{u}^\mathrm{I}(\boldsymbol{\phi}_\mathrm{u}) &= -\int_\Omega \boldsymbol{\phi}_\mathrm{u}\cdot\boldsymbol{r}\,\mathrm{d}\Omega + \int_\Gamma \boldsymbol{\phi}_\mathrm{u}\cdot\boldsymbol{t}_{\boldsymbol{n}}\,\mathrm{d}\Gamma.
\end{aligned} \tag{8}$$

The problem then becomes: Find $p_\mathrm{f}\in V_\mathrm{f}$ and $\boldsymbol{u}\in\boldsymbol{V}_\mathrm{u}$ that satisfy the following relations:

$$\begin{aligned}
a_\mathrm{f}^\mathrm{I}(\phi_\mathrm{f}, p_\mathrm{f}) + b^\mathrm{I}(\phi_\mathrm{f}, \boldsymbol{u}) &= l_\mathrm{f}^\mathrm{I}(\phi_\mathrm{f}) & \forall\phi_\mathrm{f}\in V_\mathrm{f}, \tag{9} \\
a_\mathrm{u}^\mathrm{I}(\boldsymbol{\phi}_\mathrm{u}, \boldsymbol{u}) + b^\mathrm{I}(p_\mathrm{f}, \boldsymbol{\phi}_\mathrm{u}) &= l_\mathrm{u}^\mathrm{I}(\boldsymbol{\phi}_\mathrm{u}) & \forall\boldsymbol{\phi}_\mathrm{u}\in\boldsymbol{V}_\mathrm{u}. \tag{10}
\end{aligned}$$

The normal flux $f_{\boldsymbol{n}} = \boldsymbol{v}_\mathrm{D}\cdot\boldsymbol{n}$ and normal stresses $\boldsymbol{t}_{\boldsymbol{n}}$ on the boundary Γ appear in these equations as natural boundary conditions. We note that Equations (9)–(10) form a symmetric, but indefinite, system of equations,[†] which can in principle be solved either iteratively or simultaneously (fully coupled). Dean *et al.* [12] finds the fully coupled method to be most efficient in a case with strong hydromechanical coupling, and in our experiments we have observed very slow convergence of iterative methods in problems with high permeability contrasts. Hence, we shall only consider the fully coupled method in the following.

The natural spaces for the continuous problem are $V_\mathrm{f} = H^1$ (or L^2 when $\boldsymbol{\Lambda} = 0$) for the pressure and $\boldsymbol{V}_\mathrm{u} = \boldsymbol{H}^1$ for the displacement. The discrete finite element approximation follows from solving the equations for the weak form in finite-dimensional spaces. We shall return later to the question of discrete spaces.

[†]Symmetric because the trial $(p_\mathrm{f}, \boldsymbol{u})$ and test $(\phi_\mathrm{f}, \boldsymbol{\phi}_\mathrm{u})$ functions are interchangeable; indefinite because a_f^I is negative definite while a_u^I is positive definite.

2.1. Three-field (fluid velocity) formulation

In many applications of the poroelastic equations, the flow of the fluid through the medium is of primary interest. However, due to the differential operator acting on the pressure p_f, the flow is of lower accuracy than the pressure itself. Furthermore, the derivative is not continuous between elements, and hence the fluid mass is not in general conserved. A natural extension is then to introduce $\boldsymbol{v}_\mathrm{D}$ as an extra primary variable in a mixed finite element formulation. The order of accuracy is higher, and mass conservation for the fluid phase can be ensured by using continuous elements for $\boldsymbol{v}_\mathrm{D}$.

By inserting the relation for fluid flux, Equation (3), into Equation (1), we get a coupled system of three equations (of which two are vector equations). The equations for fluid flux and pressure are

$$S\dot{p}_\mathrm{f} + \boldsymbol{\nabla} \cdot \boldsymbol{v}_\mathrm{D} + \alpha \boldsymbol{\nabla} \cdot \dot{\boldsymbol{u}} = q, \tag{11}$$

$$\boldsymbol{\Lambda}^{-1}\boldsymbol{v}_\mathrm{D} + \boldsymbol{\nabla} p_\mathrm{f} = \boldsymbol{r}_\mathrm{f}, \tag{12}$$

and these are coupled with the unmodified Equation (2) for solid displacement. We shall call this the fluid velocity three-field formulation.

Weak discrete-in-time form. We define the following additional forms:

$$\begin{aligned}
a_\mathrm{f}^\mathrm{II}(\phi_\mathrm{f}, p_\mathrm{f}) &= -\int_\Omega S\phi_\mathrm{f}p_\mathrm{f}\,\mathrm{d}\Omega, \\
b^\mathrm{II}(\phi_\mathrm{f}, \boldsymbol{v}_\mathrm{D}) &= -\int_\Omega p_\mathrm{f}\boldsymbol{\nabla} \cdot \boldsymbol{v}_\mathrm{D}\,\mathrm{d}\Omega\Delta t, \\
l_\mathrm{f}^\mathrm{II}(\phi_\mathrm{f}) &= -\int_\Omega (q\Delta t + S\hat{p}_\mathrm{f} + \boldsymbol{\nabla} \cdot \hat{\boldsymbol{u}})\phi_\mathrm{f}\,\mathrm{d}\Omega,
\end{aligned} \tag{13}$$

which are derived from Equation (11), and

$$\begin{aligned}
a_\mathrm{v}^\mathrm{II}(\boldsymbol{\phi}_\mathrm{v}, \boldsymbol{v}_\mathrm{D}) &= \int_\Omega \boldsymbol{\phi}_\mathrm{v} \cdot \boldsymbol{\Lambda}^{-1}\boldsymbol{v}_\mathrm{D}\,\mathrm{d}\Omega\Delta t, \\
c^\mathrm{II}(\boldsymbol{\phi}_\mathrm{v}, p_\mathrm{f}) &= \int_\Gamma (\boldsymbol{\phi}_\mathrm{v} \cdot \boldsymbol{n})p_\mathrm{f}\,\mathrm{d}\Gamma\Delta t, \\
l_\mathrm{v}^\mathrm{II}(\boldsymbol{\phi}_\mathrm{v}) &= \int_\Omega \boldsymbol{\phi}_\mathrm{v} \cdot \boldsymbol{r}_\mathrm{f}\,\mathrm{d}\Omega.
\end{aligned} \tag{14}$$

from Equation (12). The solution is then given as $(\boldsymbol{u}, p_\mathrm{f}, \boldsymbol{v}_\mathrm{D}) \in V = \boldsymbol{V}_\mathrm{u} \times V_\mathrm{f} \times \boldsymbol{V}_\mathrm{v}$ satisfying

$$a_\mathrm{f}^\mathrm{II}(\phi_\mathrm{f}, p_\mathrm{f}) + b^\mathrm{I}(\phi_\mathrm{f}, \boldsymbol{u}) + b^\mathrm{II}(\phi_\mathrm{f}, \boldsymbol{v}_\mathrm{D}) = l_\mathrm{f}^\mathrm{II}(\phi_\mathrm{f}) \qquad \forall \phi_\mathrm{f} \in V_\mathrm{f}, \tag{15}$$

$$a_\mathrm{v}^\mathrm{II}(\boldsymbol{\phi}_\mathrm{v}, \boldsymbol{v}_\mathrm{D}) + b^\mathrm{II}(p_\mathrm{f}, \boldsymbol{\phi}_\mathrm{v}) + c^\mathrm{II}(\boldsymbol{\phi}_\mathrm{v}, p_\mathrm{f}) = l_\mathrm{v}^\mathrm{II}(\boldsymbol{\phi}_\mathrm{v}) \qquad \forall \boldsymbol{\phi}_\mathrm{v} \in \boldsymbol{V}_\mathrm{v}, \tag{16}$$

along with Equation (10) for the displacement.

The displacement space is the same as in the two-field formulation, while the pressure space is always L^2 (in the two-field formulation, this is the case only when $\boldsymbol{\Lambda} = 0$). Additionally, we define the fluid velocity space as $\boldsymbol{V}_\mathrm{v} = \boldsymbol{H}(\mathrm{div})^\ddagger$. We note that the system is symmetric only when $c^\mathrm{II} = 0$; this is achieved when the whole boundary has either zero fluid pressure or zero fluid flux conditions (and the spaces V_f and $\boldsymbol{V}_\mathrm{v}$ are restricted accordingly).

2.2. Three-field (solid pressure) formulation

In the field of (pure) elasticity, it is well understood that a low-compressible material (with Poisson's ratio close to 0.5) leads to unphysical oscillations in the solid pressure field, and in some cases also to

---

$\ddagger \boldsymbol{L}^2 \supset \boldsymbol{H}(\mathrm{div}) = \{\boldsymbol{v} \in \boldsymbol{L}^2 \mid \boldsymbol{\nabla} \cdot v \in L^2\} \supset \boldsymbol{H}^1 = \{\boldsymbol{v} \in \boldsymbol{L}^2 \mid \boldsymbol{\nabla}v \in \mathbf{L}^2\}$

Prepared using **nagauth.cls**

a wrong solution for the calculated displacement. This can be explained by λ becoming very large in
Equation (2), leading to the requirement that $\boldsymbol{\nabla} \cdot \boldsymbol{u} \to 0$. When this requirement is applied to standard
finite elements, several degrees of freedom become "locked", leaving too few degrees of freedom to
represent the correct solution.

One way to overcome this obstacle is to introduce a new primary variable for the solid pressure. We
define the (incomplete) solid pressure as

$$\overline{p}_{\mathrm{s}} = -\lambda \boldsymbol{\nabla} \cdot \boldsymbol{u}, \tag{17}$$

whereby Equation (2) can be rewritten as the coupled equations,

$$\boldsymbol{\nabla}\mu\boldsymbol{\nabla} \cdot \boldsymbol{u} + \boldsymbol{\nabla} \cdot \mu\boldsymbol{\nabla}\boldsymbol{u} - \boldsymbol{\nabla}\overline{p}_{\mathrm{s}} - \alpha\boldsymbol{\nabla}p_{\mathrm{f}} = \boldsymbol{r}, \tag{18}$$

$$\lambda^{-1}\overline{p}_{\mathrm{s}} + \boldsymbol{\nabla} \cdot \boldsymbol{u} = 0, \tag{19}$$

and combined with Equation (1) for the fluid pressure. This definition of the solid pressure makes the
equation simpler than when using the volumetric solid stress, $p_{\mathrm{s}} = -\sigma_{\mathrm{vol}} = -(\lambda + \frac{2}{3}\mu)\boldsymbol{\nabla} \cdot \boldsymbol{u}$, while
still including the "difficult" part of the pressure.

The three-field (solid pressure) formulation can be used with low-compressible or even
incompressible materials.

Weak discrete-in-time form.   The additional variational forms associated with Equations (18)–(19) are

$$\begin{aligned}
a_{\mathrm{u}}^{\mathrm{III}}(\boldsymbol{\phi}_{\mathrm{u}}, \boldsymbol{u}) &= \int_{\Omega} \mu\boldsymbol{\nabla}\boldsymbol{\phi}_{\mathrm{u}} : \boldsymbol{\nabla}\boldsymbol{u}\,\mathrm{d}\Omega, \\
a_{\mathrm{s}}^{\mathrm{III}}(\phi_{\mathrm{s}}, \overline{p}_{\mathrm{s}}) &= \int_{\Omega} \lambda^{-1}\phi_{\mathrm{s}}\overline{p}_{\mathrm{s}}\,\mathrm{d}\Omega, \\
b^{\mathrm{III}}(\phi_{\mathrm{s}}, \boldsymbol{u}) &= \int_{\Omega} \phi_{\mathrm{s}}\boldsymbol{\nabla} \cdot \boldsymbol{u}\,\mathrm{d}\Omega,
\end{aligned} \tag{20}$$

and the solution is given as $(\boldsymbol{u}, \overline{p}_{\mathrm{s}}, p_{\mathrm{f}}) \in \boldsymbol{V}_{\mathrm{u}} \times V_{\mathrm{s}} \times V_{\mathrm{f}}$ satisfying

$$a_{\mathrm{u}}^{\mathrm{III}}(\boldsymbol{\phi}_{\mathrm{u}}, \boldsymbol{u}) + b^{\mathrm{I}}(p_{\mathrm{f}}, \boldsymbol{\phi}_{\mathrm{u}}) + b^{\mathrm{III}}(\overline{p}_{\mathrm{s}}, \boldsymbol{\phi}_{\mathrm{u}}) = l_{\mathrm{u}}^{\mathrm{I}}(\boldsymbol{\phi}_{\mathrm{u}}) \qquad \forall\boldsymbol{\phi}_{\mathrm{u}} \in \boldsymbol{V}_{\mathrm{u}}, \tag{21}$$

$$a_{\mathrm{s}}^{\mathrm{III}}(\phi_{\mathrm{s}}, \overline{p}_{\mathrm{s}}) + b^{\mathrm{III}}(\phi_{\mathrm{s}}, \boldsymbol{u}) = 0 \qquad \forall\phi_{\mathrm{s}} \in V_{\mathrm{s}}, \tag{22}$$

along with the original equation for the fluid pressure, Equation (9). The continuous spaces are as in
the two-field formulation, with the addition of the solid pressure space $V_{\mathrm{s}} = L^2$.

2.3. Four-field formulation

Combining the three-field formulations of fluid velocity and solid pressure, we get a formulation of two
scalar and two vector fields which attains accurate fluid velocities, and which is stable in the presence of
low-compressible materials. The formulation is obtained as the coupled system of Equations (11)–(12)
and (18)–(19), as

$$S\dot{p}_{\mathrm{f}} + \boldsymbol{\nabla} \cdot \boldsymbol{v}_{\mathrm{D}} + \alpha\boldsymbol{\nabla} \cdot \dot{\boldsymbol{u}} = q, \tag{23}$$

$$\boldsymbol{\Lambda}^{-1}\boldsymbol{v}_{\mathrm{D}} + \boldsymbol{\nabla}p_{\mathrm{f}} = \boldsymbol{r}_{\mathrm{f}}, \tag{24}$$

$$\boldsymbol{\nabla}\mu\boldsymbol{\nabla} \cdot \boldsymbol{u} + \boldsymbol{\nabla} \cdot \mu\boldsymbol{\nabla}\boldsymbol{u} - \boldsymbol{\nabla}\overline{p}_{\mathrm{s}} - \alpha\boldsymbol{\nabla}p_{\mathrm{f}} = \boldsymbol{r}, \tag{25}$$

$$\lambda^{-1}\overline{p}_{\mathrm{s}} + \boldsymbol{\nabla} \cdot \boldsymbol{u} = 0, \tag{26}$$

Weak discrete-in-time form.   The weak form of the four-field formulation is: Find $(\boldsymbol{u}, \boldsymbol{v}_{\mathrm{D}}, p_{\mathrm{f}}, \overline{p}_{\mathrm{s}}) \in \boldsymbol{V}_{\mathrm{u}} \times \boldsymbol{V}_{\mathrm{v}} \times V_{\mathrm{f}} \times V_{\mathrm{s}}$ such that Equations (15)–(16) and Equations (21)–(22) are satisfied.

(a) The two-material problem

(b) Oscillatory solution to the two-material problem with uniform load; $F = 1$, $\epsilon = 10^{-8}$, $\Delta t = 1$.
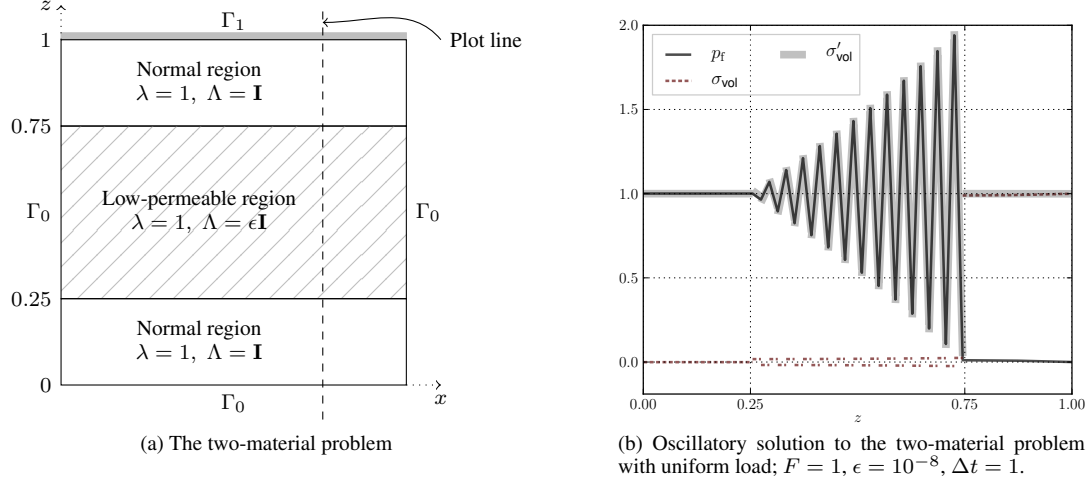
Figure 1: Domain for illustrating pressure oscillations. On the sides and bottom, no-flux conditions are imposed so that no fluid or solid movement is allowed in the normal direction. The top is drained with fluid pressure $p_f = 0$ and an applied normal stress. Spurious pressure oscillations are clearly present in (b) — the analytical solution is constant $\sigma'_{\text{vol}} = 1$.

3. On the causes of pressure oscillations

It is well known that spurious fluid pressure oscillations may occur in low-permeable regions in finite element calculations of the poroelastic equations [10, 13, 14]. To illustrate this phenomenon, we use a simple test case where a low-permeable layer is placed inside a "normal" material, shown in Figure 1a. The low-permeable layer uses $\Lambda = \epsilon \mathbf{I}$ for some $\epsilon \ll 1$, while the "normal" layer has unit permeability. In all three layers, the elastic parameters are set to $\lambda = \mu = 1$. The boundary conditions at the sides and bottom are no-flux for both the fluid and the solid,

$$f_{\boldsymbol{n}}|_{\Gamma_0} = 0, \qquad \boldsymbol{u} \cdot \boldsymbol{n}|_{\Gamma_0} = 0, \tag{27}$$

while the top boundary is drained, with an applied normal force

$$p_f|_{\Gamma_1} = 0, \qquad \boldsymbol{t}_{\boldsymbol{n}}|_{\Gamma_1} = F(x)\boldsymbol{n}, \tag{28}$$

where $F(x)$ is constant 1 for the present. No body forces are present, and the initial conditions are $\boldsymbol{u} = 0$ and $p_f = 0$ with $\Delta t = 1$.

Figure 1b shows the naïve numerical solution to the two-material test case when ϵ is very small, computed with the two-field formulation using first order quadrilateral elements $(Q_1/Q_1)^{\S}$. The pressure oscillations in the middle layer clearly have no physical basis, nor are they present in the analytical solution to the problem.

[§]Elements are listed in the order $\boldsymbol{u}\bar{p}_{\text{s}}/\boldsymbol{v}_{\text{D}}p_{\text{f}}$, where any unused position for a particular formulation is skipped. Hence, the two-field formulation uses $\boldsymbol{u}/p_{\text{f}}$, fluid velocity three-field uses $\boldsymbol{u}/\boldsymbol{v}_{\text{D}}p_{\text{f}}$, and solid pressure three-field uses $\boldsymbol{u}\bar{p}_{\text{s}}/p_{\text{f}}$.

(a) The Barry-Mercer problem.

(b) Oscillatory solution to the Barry-Mercer problem, with $\epsilon = 10^{-8}$, $\Delta t = 0.01$.
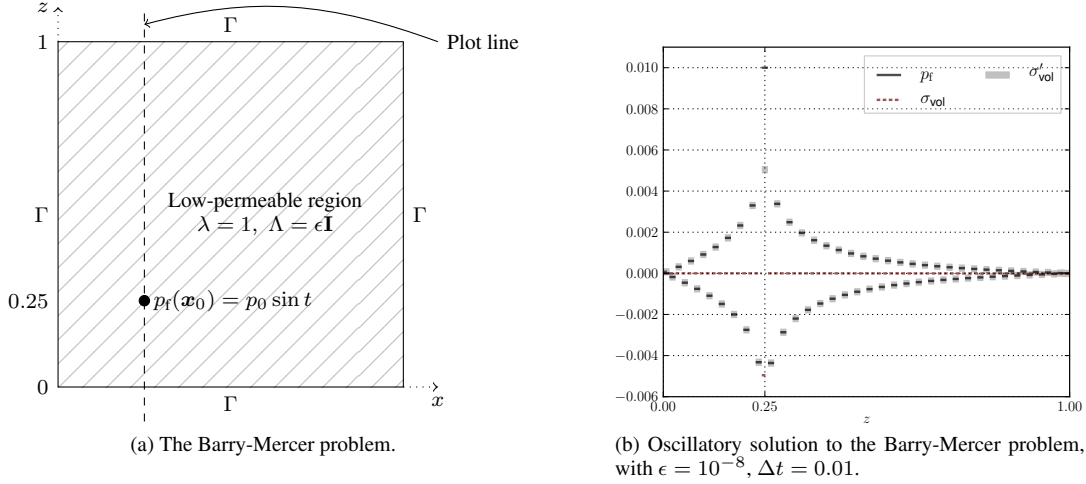
Figure 2: The Barry-Mercer problem consists of a pulsating pressure point source embedded in a uniform porous material which is drained on all sides, with zero tangential displacement. Pressure oscillations are clearly visible when using $Q_1/\mathrm{RT}_1 Q_0$ elements.

Studying the fluid velocity three-field formulation, Phillips and Wheeler [13] argue that such pressure oscillations have the same cause as the phenomenon known as locking in pure elasticity. To see why, we consider that the basic linear elastic equation is just Equation (2) without the fluid pressure term,

$$\boldsymbol{\nabla}(\lambda + \mu)\boldsymbol{\nabla} \cdot \boldsymbol{u} + \boldsymbol{\nabla} \cdot \mu\boldsymbol{\nabla}\boldsymbol{u} = \boldsymbol{r}. \tag{29}$$

Elastic locking occurs when finite elements are asked to reproduce a displacement field that is nearly divergence free, as $\lambda \to \infty$ corresponds to $\boldsymbol{\nabla} \cdot \boldsymbol{u} \to 0$. Satisfying this with standard (low-order piecewise polynomial) finite elements locks out many of the degrees of freedom, to the extent that only constant displacement fields can be represented. More commonly, the error in displacement is seen to cause nonphysical oscillations in the solid pressure ($p_\mathrm{s} \to \overline{p}_\mathrm{s} = -\lambda\boldsymbol{\nabla} \cdot \boldsymbol{u}$). This is because the errors in $\boldsymbol{\nabla} \cdot \boldsymbol{u} \approx 0$ are magnified by a very large factor λ in the post-process calculation of the volumetric stress.

The argument by Phillips and Wheeler is that under certain conditions the same happens in poroelasticity. Consider Equation (1) with uniform permeability, discretised in time with time step Δt and with $S = q = 0$. Assume furthermore that we take one time step from a divergence-free initial state, which is quite normal at the start of a simulation (when $\boldsymbol{u} = 0$). Then, Equation (1) reduces to

$$\boldsymbol{\nabla} \cdot \boldsymbol{u} = \Delta t \boldsymbol{\nabla} \cdot \boldsymbol{\Lambda}\boldsymbol{\nabla} p_\mathrm{f}/\alpha, \tag{30}$$

The right-hand side becomes very small for short time steps and low permeabilities. Again, the requirement for a nearly divergence-free solution for the displacement $\boldsymbol{u}$ appears. Fluid pressure oscillations are demonstrated in (among others) the Barry-Mercer problem (shown in Figure 2a), using the three-field formulation with lowest-order Raviart-Thomas elements for the fluid and linear elements for the displacement ($Q_1/\mathrm{RT}_1 Q_0$). This problem [15] consists of a pulsating pressure point source embedded in a uniform porous material, with boundary conditions chosen to permit an analytical

(a) $\epsilon = 10^{-1}$ (b) $\epsilon = 10^{-4}$ (c) $\epsilon = 10^{-8}$
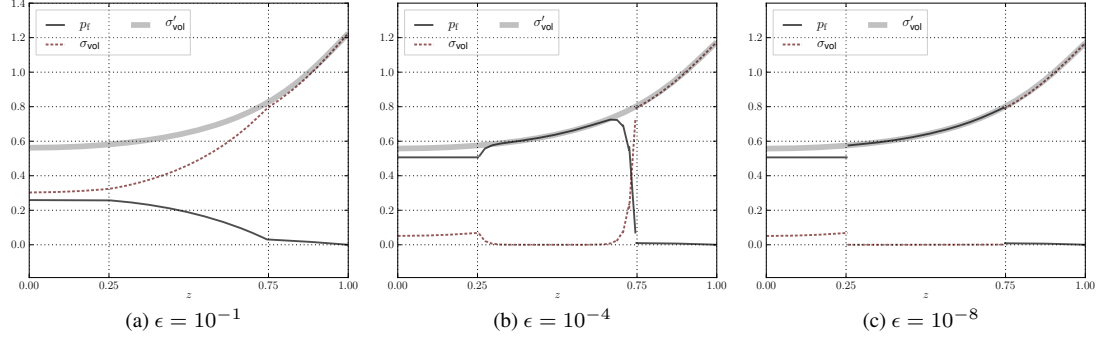
Figure 3: Plausible (smooth) solution for the three-material problem with a low-permeable layer and non-uniform load. As ϵ decreases, the fluid pressure becomes dominant in the middle layer, and each of the pressure components approach a discontinuous solution.

solution: $p_f|_\Gamma = 0$, $\boldsymbol{u} \times \boldsymbol{n}|_\Gamma = 0$, and initial conditions $\boldsymbol{u} = 0$ and $p_f = 0$. The pressure oscillations disappear when the displacement is instead calculated with a discontinuous Galerkin method, and the optimality of the pressure solution is proven for this method.

As regards the test case shown in Figure 1, we remark that elastic locking can not appear in this test case which is one-dimensional, because in one dimension $\boldsymbol{\nabla} \cdot \boldsymbol{u} = \partial \boldsymbol{u}_x / \partial x \to 0$ implies constant displacement — a trivial solution which can be represented by any element. Hence, the oscillations shown in this figure are *not* caused by elastic locking.

We therefore introduce asymmetry through a load on just the right half of the top boundary, $F(x) = \{0$ when $x < 0.5$, 1 otherwise$\}$, in the three-layer problem (Figure 1a). With asymmetric loading we do not have an analytical solution, unlike in the uniform-load case. Instead, we use the fact that the volumetric effective stress,

$$\sigma'_{\text{vol}} = \frac{\text{Tr}\,\sigma'}{3} = \overline{p}_s + \frac{2}{3}\mu \boldsymbol{\nabla} \cdot \boldsymbol{u} + \alpha p_f, \tag{31}$$

should be continuous and smooth (away from the externally applied discontinuity on the surface at $x = 0.5$). The solution is illustrated in Figure 3, where the thick gray line shows that σ'_{vol} is continuous even when each of its three components is discontinuous. The smoothness of σ'_{vol} does not prove that the numerical solution converges, but it makes it easy to identify many of the wrong solutions with oscillating pressure.¶ In the text, we refer to these apparently correct solutions as "plausible", since they are not compared to a known analytical solution.

We now compare the behaviour of the non-uniform load problem with a low-permeable layer to that of a low-compressible layer. In the latter case, the middle layer of Figure 1a is replaced with a layer

---

¶We also note that the existence of analytical solutions is no panacea. As noted in, e.g., [16], geologically relevant solutions are often not realisable on a reasonably sized computational mesh. For example, the fluid pressure solution in Figure 1b should have a very sharp gradient between the two top layers, a feature that is not possible to realise with continuous elements unless an extremely fine grid is used. Similarly, the Barry-Mercer problem requires a point pressure source, while discrete analogues have source areas on the order of the element size. These inaccuracies in the discrete model may mask any "real" convergence difficulties for all but very fine meshes.
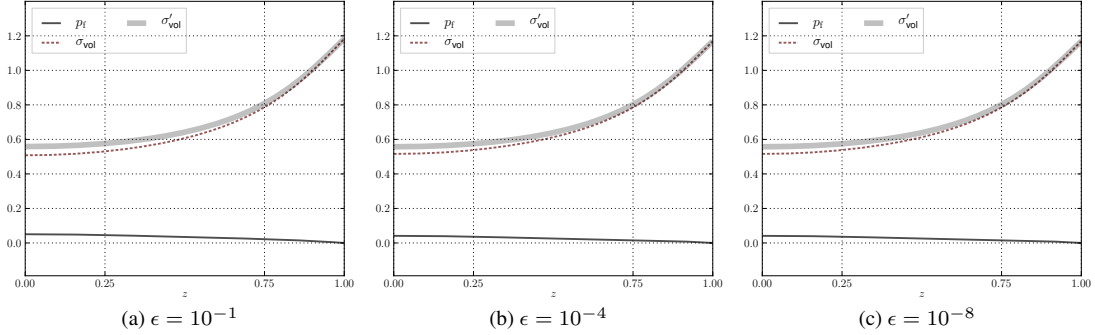
Figure 4: Plausible (smooth) solution for the three-material problem with a low-compressible layer and non-uniform load. As opposed to the low-permeable case in Figure 3, the pressure components are continuous.

with unit permeability but low compressibility; $\lambda = \epsilon^{-1}$, $\mathbf{\Lambda} = \mathbf{I}$. The plausible (smooth) solution to this problem is shown in Figure 4. The total pressure profile is similar to the low-permeable problem, but the load in the middle layer is here mainly supported by the volumetric stress, instead of the fluid pressure. Furthermore, we know that this problem is susceptible to elastic locking. Figure 5 compares these two cases using equal-order Q_1/Q_1 elements. As expected, the low-permeable problem has difficulty with the fluid pressure, while the low-compressible problem has difficulty with the volumetric stress. There is, however, a major difference in the effect that this has on the displacement. Figure 6 compares the locking behaviour of the low-permeable and the low-compressible problems. In the low-compressible problem, the faulty pressure is associated with elastic locking, i.e., the displacement is pulled toward a constant in the middle region, Figure 6b. This restriction of the displacement is not seen in the low-permeable problem, Figure 6a.

It appears that elastic locking is not in general a sufficient explanation for the fluid pressure oscillations in low-permeable regions.

4. Spurious pressure oscillations and saddle-point problems

It is instructive to look at the case of total impermeability, $\mathbf{\Lambda} = S = 0$. For clarity of presentation, we furthermore set $\alpha = 1$ and let $\tilde{q} = q\Delta t + \mathbf{\nabla} \cdot \hat{\boldsymbol{u}}$, where $\hat{\boldsymbol{u}}$ is the value of $\boldsymbol{u}$ at the previous time step. In this case, Equations (1)–(2)[||] take on almost the same form as those of the *mixed* formulation of incompressible linear elasticity (as opposed to the pure displacement formulation mentioned in the previous section). This is evident when we compare the impermeable poroelastic equations

$$\mathbf{\nabla}(\lambda + \mu)\mathbf{\nabla} \cdot \boldsymbol{u} + \mathbf{\nabla} \cdot \mu\mathbf{\nabla}\boldsymbol{u} - \mathbf{\nabla}p_{\mathrm{f}} = \boldsymbol{r}, \qquad\qquad \mathbf{\nabla} \cdot \boldsymbol{u} = \tilde{q}, \qquad (32)$$

[||] Or Equations (11)–(12) and (2) after eliminating $\boldsymbol{v}_{\mathrm{D}} = 0$.
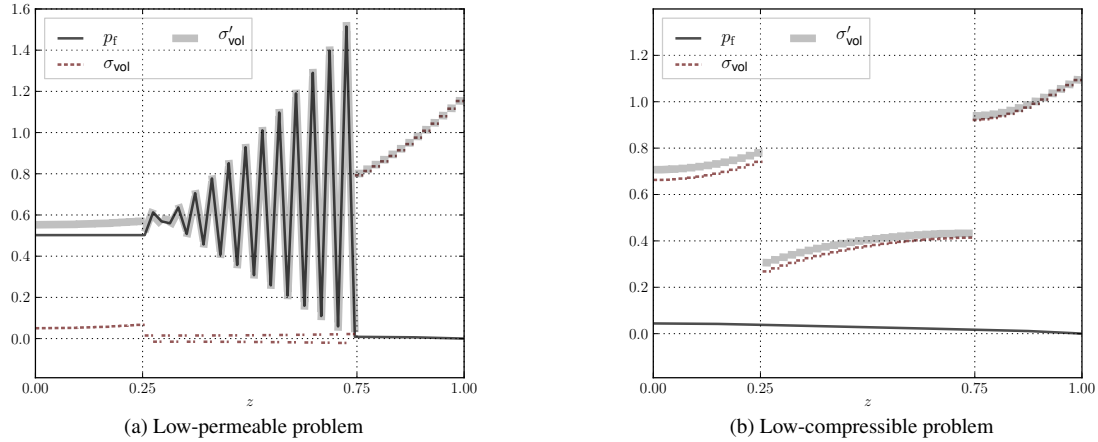
(a) Low-permeable problem

(b) Low-compressible problem

Figure 5: Comparison of the two-field (Q_1/Q_1) solutions for a low-permeable and a low-compressible layer. The solutions are erroneous for the fluid pressure in (a) and for the volumetric stress in (b). With this particular choice of elements (and problem geometry), the volumetric stress does not oscillate, but the error is still obvious as an abrupt drop in σ'_{vol}. The corresponding plausible pressure solutions are shown in Figure 3c for (a), and in Figure 4c for (b).

(a) Low-permeable problem

(b) Low-compressible problem
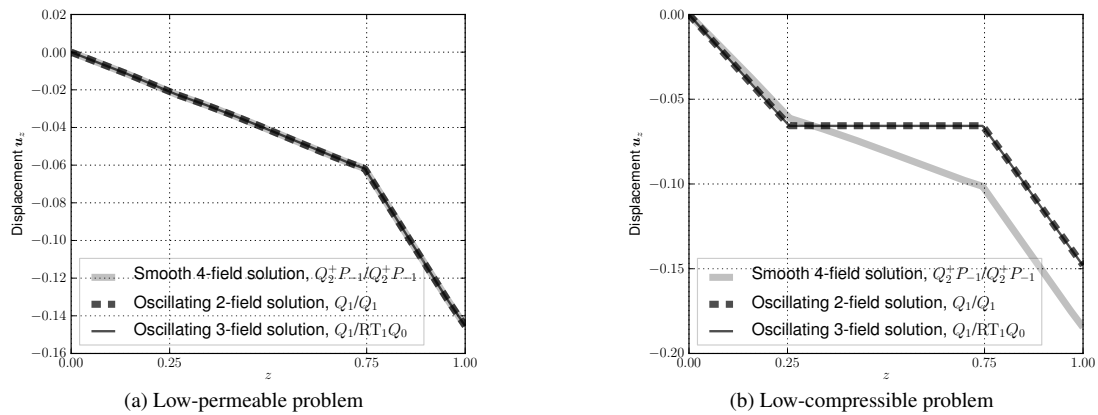
Figure 6: Comparison of the vertical displacement with non-uniform load. Notice the nearly constant displacement in the low-compressible layer in (b), while the low-permeable layer does not lock the displacement (a). $\epsilon = 10^{-8}$

with the incompressible elastic equations

$$\nabla\mu\nabla\cdot\boldsymbol{u} + \nabla\cdot\mu\nabla\boldsymbol{u} - \nabla\bar{p}_{\mathrm{s}} = \boldsymbol{r}, \qquad \nabla\cdot\boldsymbol{u} = 0. \qquad (33)$$

Much of the analysis of Equation (33) is valid also for the present problem. In particular, Bathe [11] notes that the weak form of Equation (33) has two major failure modes: The first is the already mentioned elastic locking, wherein the displacement space is overly constrained by $\nabla\cdot\boldsymbol{u} = 0$. The second failure mode occurs when the pressure space is too large and contains spurious pressure modes.

In linear algebra terms, Equation (33) can be discretised as

$$\begin{bmatrix} A & B \\ B^{\mathsf{T}} & 0 \end{bmatrix} \begin{bmatrix} \mathrm{u} \\ \mathrm{p_s} \end{bmatrix} = \begin{bmatrix} \mathrm{r} \\ 0 \end{bmatrix}, \qquad (34)$$

where $B_{ij} = b^{\mathrm{I}}(\phi_{\mathrm{s}}^{j}, \phi_{\mathrm{u}}^{i})$ (and $\boldsymbol{u}$ is approximated as $\boldsymbol{u}_h = \sum_k \mathrm{u}^k\phi_{\mathrm{u}}^k$; similarly for p). Then, locking follows when $\mathrm{kernel}(B^{\mathsf{T}})$ does not span the displacement space, while spurious pressure modes are a consequence of a too large $\mathrm{kernel}(B)$. The same argument can be used in the poroelastic case, Equation (32), except that the presence of locking is now determined by the space spanned by solutions of $B^{\mathsf{T}}\mathrm{u} = \tilde{\mathrm{q}}$ instead of the null space.

If the cause of the fluid pressure oscillations lies in the well-posedness of the discrete weak form of the equations, we know from, e.g., [17], that the solvability of the equations and the stability of the solution follows from the Babuška inf-sup condition [18], which should be fulfilled for any mesh size h:

$$\gamma_0 \le \gamma_h = \inf_{v_h\in V_h}\sup_{w_h\in V_h}\frac{|c(v_h, w_h)|}{\|v_h\|_V\|w_h\|_V}, \qquad (35)$$

for some $\gamma_0 > 0$. In the four-field formulation, for example, the discrete space is $V_h = \boldsymbol{V}_{\mathrm{u}}\times V_{\mathrm{f}}\times\boldsymbol{V}_{\mathrm{v}}\times V_{\mathrm{s}}$ and v_h, w_h are functions in this space, e.g., $v_h = (v_{\boldsymbol{u}}, v_{p_{\mathrm{f}}}, v_{\boldsymbol{v}_{\mathrm{D}}}, v_{\bar{p}_{\mathrm{s}}}) \in V_h$. The key insight is that this condition must be fulfilled for the complete coupled system of equations, and not only separately for the fluid velocity/fluid pressure and the solid displacement/solid pressure. Hence, c in Equation (35) is defined as

$$c(\boldsymbol{\phi}, \boldsymbol{\psi}) = a_{\mathrm{f}}^{\mathrm{II}}(\phi_f, \psi_f) + a_{\mathrm{v}}^{\mathrm{II}}(\phi_v, \psi_v) + a_{\mathrm{u}}^{\mathrm{III}}(\phi_u, \psi_u) + a_{\mathrm{s}}^{\mathrm{III}}(\phi_s, \psi_s) + b^{\mathrm{I}}(\phi_f, \psi_u)$$
$$+ b^{\mathrm{II}}(\phi_f, \psi_v) + b^{\mathrm{II}}(\psi_f, \phi_v) + c^{\mathrm{II}}(\phi_v, \psi_f) + b^{\mathrm{I}}(\psi_f, \phi_u) + b^{\mathrm{III}}(\psi_s, \phi_u) + b^{\mathrm{III}}(\phi_s, \psi_u). \quad (36)$$

In the special case of symmetric saddle-point problems, on the canonical form $a(v, u) + b(v, p) + b(u, q) = l((v, q))$, $\forall(v, q) \in V$ and with a coercive, the following Brezzi conditions [17] are equivalent to the Babuška condition. The Brezzi coercivity constant α_h is

$$\alpha_h = \inf_{u\in Z_h}\sup_{v\in Z_h}\frac{a(u, v)}{\|u\|_V\|v\|_V}, \qquad (37)$$

with $Z_h = \{v \in V_h \,|\, b(v, q) = 0, \ \forall q \in Q_h\}$, while the Brezzi inf-sup constant** β_h is

$$\beta_h = \inf_{q\in Q_h}\sup_{v\in V_h}\frac{b(v, q)}{\|v\|_V\|q\|_Q} \qquad (38)$$

**The Brezzi inf-sup condition is also known as the Ladyzhenskaya-Babuška-Brezzi (LBB) condition.

Copyright © 2000 John Wiley & Sons, Ltd.
Prepared using nagauth.cls

Int. J. Numer. Anal. Meth. Geomech. 2000; **0**:0–0

Both of these should be bounded from below as $h \to 0$. The Brezzi inf-sup constant is particularly interesting, because zero values for β_h indicate the presence of spurious modes in Q_h (as we stated in terms of the kernel of the matrix B in the previous section).

The two-field formulation approaches a saddle-point problem when $S = 0$ and $\Lambda \to 0$, in which case it is similar to the mixed linear elasticity problem (for finite λ). Spurious pressure modes are then associated with zero values of the Brezzi inf-sup constant,

$$\beta_h = \inf_{q \in V_f} \sup_{\boldsymbol{v} \in \boldsymbol{V}_u} \frac{b^{\mathrm{I}}(q, \boldsymbol{v})}{\|q\|_{V_f} \|\boldsymbol{v}\|_{\boldsymbol{V}_u}}. \tag{39}$$

The three-field (fluid velocity) problem, however, is a true saddle-point problem whenever $S = 0$ (and symmetric when $c^{\mathrm{II}} = 0$). We can define

$$a((\boldsymbol{v}, \boldsymbol{w}), (\boldsymbol{x}, \boldsymbol{y})) = a_u^{\mathrm{I}}(\boldsymbol{v}, \boldsymbol{x}) + a_v^{\mathrm{II}}(\boldsymbol{w}, \boldsymbol{y}), \tag{40}$$

$$b(q, (\boldsymbol{v}, \boldsymbol{w})) = b^{\mathrm{I}}(q, \boldsymbol{v}) + b^{\mathrm{II}}(q, \boldsymbol{w}), \tag{41}$$

$$l((p, \boldsymbol{v})) = l_u^{\mathrm{I}}(\boldsymbol{v}) + l_f^{\mathrm{II}}(p), \tag{42}$$

and restate Equations (10) and (15)–(16) in the form of a canonical saddle-point problem: Find the solution $(\boldsymbol{u}, \boldsymbol{v}_{\mathrm{D}}, p_f) \in V$ satisfying

$$a((\boldsymbol{v}, \boldsymbol{w}), (\boldsymbol{u}, \boldsymbol{v}_{\mathrm{D}})) + b(p_f, (\boldsymbol{v}, \boldsymbol{w})) + b(q, (\boldsymbol{u}, \boldsymbol{v}_{\mathrm{D}})) = l((q, \boldsymbol{v})), \quad \forall (\boldsymbol{v}, \boldsymbol{w}, q) \in V, \tag{43}$$

with Brezzi stability constants

$$\alpha_h = \inf_{(\boldsymbol{v}, \boldsymbol{w}) \in Z_h} \sup_{(\boldsymbol{x}, \boldsymbol{y}) \in Z_h} \frac{a_u^{\mathrm{I}}(\boldsymbol{v}, \boldsymbol{x}) + a_v^{\mathrm{II}}(\boldsymbol{w}, \boldsymbol{y})}{(\|\boldsymbol{v}\|_{\boldsymbol{V}_u} + \|\boldsymbol{w}\|_{\boldsymbol{V}_v})(\|\boldsymbol{x}\|_{\boldsymbol{V}_u} + \|\boldsymbol{y}\|_{\boldsymbol{V}_v})}, \tag{44}$$

$$\beta_h = \inf_{q \in V_f} \sup_{(\boldsymbol{v}, \boldsymbol{w}) \in \boldsymbol{V}_u \times \boldsymbol{V}_v} \frac{b^{\mathrm{I}}(q, \boldsymbol{v}) + b^{\mathrm{II}}(q, \boldsymbol{w})}{\|q\|_{V_f}(\|\boldsymbol{v}\|_{\boldsymbol{V}_u} + \|\boldsymbol{w}\|_{\boldsymbol{V}_v})}. \tag{45}$$

The Brezzi inf-sup constant is therefore zero only when the individual terms b^{I} and b^{II} are. These individual couplings between the variables are similar to those of well-known problems, which have known stable choices of finite element spaces:

- The displacement-fluid pressure coupling is similar to the displacement-*solid* pressure coupling in the mixed linear elasticity problem (as shown),
- the displacement-solid pressure coupling is the same as in the mixed linear elasticity problem, and
- the fluid velocity-fluid pressure coupling is same as the Darcy flow problem.

The separation of the coupling terms in the Brezzi inf-sup condition motivates our strategy of choosing combinations of element spaces that satisfy these individual problems. Hence, p_f should be chosen to be an element that is usable for mixed formulations of both linear elasticity and fluid flow. For example, if an element combination that is stable for mixed linear elasticity is chosen for $\boldsymbol{u}$ and $\overline{p}_s$, and a combination that is stable for Darcy flow is chosen for $\boldsymbol{v}_{\mathrm{D}}$ and p_f, we must then ensure that the resulting combination for $\boldsymbol{u}$ and p_f is also stable for mixed linear elasticity. An example of a combination that could work is the lowest order Raviart-Thomas (RT) for $\boldsymbol{v}_{\mathrm{D}}$-$p_f$ and the lowest order Crouzeix-Raviart (CR) or Rannacher-Turek (TR) elements for $\boldsymbol{u}$-$\overline{p}_s$. Both pressure elements (fluid and solid) are then piecewise constant, so the $\boldsymbol{u}$-p_f combination is also potentially stable (CR or TR).

With these guidelines, we proceed to examine the stability of a number of combinations of finite elements.

Copyright © 2000 John Wiley & Sons, Ltd.
Prepared using nagauth.cls

Int. J. Numer. Anal. Meth. Geomech. 2000; **0**:0–0

Table I: Summary of pairwise element combinations. Elements of polynomial order k are classified as P_k or Q_k for Lagrangian elements, while RT_k, CR_k and TR_k are the Raviart-Thomas, Crouzeix-Raviart (triangular) and Rannacher-Turek (quadrilateral) non-conforming elements, respectively. Discontinuous elements are marked as "$_{-k}$" (except $k = 0$, where this is implicit). Enriched (bubble) elements are marked by "$^{+}$".

(a) Triangular elements

Element	Comment
$P_1 P_1$	Equal order Lagrange (lowest order)
$P_2 P_2$	Equal order Lagrange
$RT_1 P_0$	Lowest order Raviart-Thomas (Hdiv) vector element
$P_2^+ P_1$	"Good element" (M. Fortin, via [22])
$P_2 P_1$	Lowest order Taylor-Hood
$P_2 P_0$	Only linear convergence in P_2 [23]
$CR_1 P_0$	Lowest order Crouzeix-Raviart non-conforming element
$P_2^+ P_{-1}$	From [23]; "optimal" [11], "good element" (M. Fortin, via [22])
$P_1^+ P_1$	MINI [24]

(b) Quadrilateral elements

Element	Comment
$Q_1 Q_1$	Equal order Lagrange (lowest order)
$Q_2 Q_2$	Equal order Lagrange
$RT_1 Q_0$	Lowest order Raviart-Thomas (Hdiv) vector element
$Q_2 Q_1$	Lowest order Taylor-Hood
$Q_2 Q_0$	Only linear convergence in Q_2
$TR_1 Q_0$	Lowest order Rannacher-Turek non-conforming
$Q_1 Q_0$	One of the most popular elements in practice [22], LBB unstable (but still usable)
$Q_2 P_{-1}$	Discontinuous, linear (rather than bi-linear) pressure; "optimal" [11], "most accurate 2D element" [22]
$Q_1^{++} Q_1$	Quadrilateral MINI analogue [25]

5. Convergence testing

The Babuška or Brezzi conditions require careful work to evaluate analytically, even for a single element family on a two-field problem. For a large number of combinations on three- and four-field problems, it is impractical. As an alternative, the conditions may be tested numerically on a series of meshes, by solving the generalised eigenvalue problems associated with the Babuška or Brezzi conditions [19, 20]. Automated tools are available for this purpose, e.g, ASCoT [21]. The full generality with regards to element definitions and boundary conditions is however not yet achieved. Hence, we have chosen to analyse the element combinations by investigating their real performance on a number of concrete test cases.

We have selected several element pairs, listed in Table I, that are in common use, and tested combinations of these. Using the four-field formulation as an example, we could choose these element pairs: $RT_1 Q_0$ for $\boldsymbol{v}_D$-p_f and $Q_2 P_{-1}$ for $\boldsymbol{u}$-$\overline{p}_s$, resulting in $Q_2 Q_0$ for $\boldsymbol{u}$-p_f. This is written as the element combination $Q_2 P_{-1}/RT_1 Q_0$.

Two of the test cases are as described earlier: A problem with a low-permeable layer embedded in a normal one from Figure 1a, and the Barry-Mercer problem, with a point pressure source inside a low-permeable material from Figure 2a. For the Barry-Mercer problem, we use elastic parameters $\lambda = \mu = 1$, a time step of $\Delta t = 0.01$, and source strength $p_0 = 1$.

The third test case is shown in Figure 7a. It is a variation of the earlier embedded-layer case, where the top layer is made low-compressible. Thus, there are three layers: The top one low-compressible; the middle one low-permeable; and the bottom one normal. The two three-layer cases are both tested with uniform load and with load on just the right half of the top boundary.
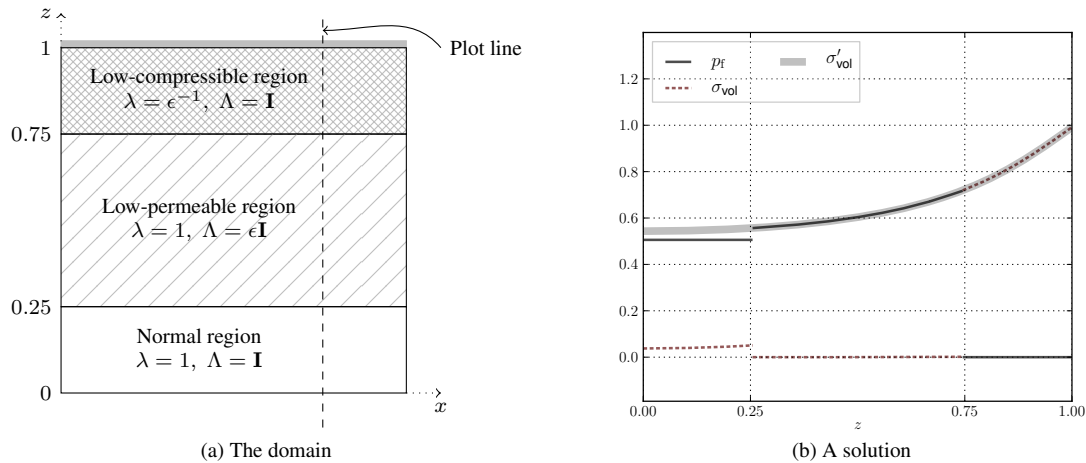
Figure 7: The three-material test case. In the top layer, the load is carried by the solid pressure; in the middle layer by the fluid pressure.

In either case, we evaluate the solution after a single time step. As reported in, e.g., [6], the pressure oscillations tend to smooth out over time, and hence the first time step is the most revealing one.

We have summarised the results in Table II. Most of the results are as expected based on our previous analysis: The equal interpolation elements, and those which are picked from known-stable pairs in Table I mostly work. The exceptions are the CR_1P_0 and TR_1Q_0 non-conforming elements for $\boldsymbol{u}$-p_f. The CR_1 or TR_1 element might potentially be useful for $\boldsymbol{u}$ when using RT_1 for $\boldsymbol{v}_D$, since both are first order and both combine with piecewise constant pressure elements. As noted in the table, we were able to "fix" the TR_1 element by setting extra tangential boundary conditions, but this solution is not very satisfactory in general.

The Q_1/RT_1Q_0 combination for the fluid velocity three-field formulation succeeds with the two- and three-material problems, but fails on the Barry-Mercer problem. The latter failure is shown in figure Figure 2b, which illustrates what is called the "checkerboard" spurious pressure mode (as does Figure 1b). This spurious mode is well known and ubiquitous [11, 22]. It can in many cases be "fixed" by juggling of boundary conditions; in particular, by releasing tangential essential conditions. Furthermore, Gresho and Sani [22] state that in their experience (and analysis) the Q_1Q_0 combination actually has optimal convergence after filtering the spurious pressure modes.

Whenever the domain has large permeability contrasts, the solution may contain steep pressure gradients. Discontinuous elements may then be advantageous to avoid localised oscillations in the fluid pressure. Comparing Figure 8a and Figure 8b, it is evident that the continuous pressure elements cannot represent the gradient at the interface between the high- and low-permeable region, and the resulting overshoot induces local oscillations in the pressure solution. When using discontinuous elements for the fluid pressure, these oscillations are not present. Discontinuous elements for the fluid pressure can not be used in the two-field formulation, where H^1 regularity is required.

Nevertheless, local pressure oscillations may still occur in certain situations, for example in early times of the Terzaghi consolidation problem. Terzaghi's problem, analysed in for example [26], describes the vertical consolidation of saturated soil. One end of the soil column is drained, and a

Table II: Summary of the numerical stability results for different elements. The test cases are (in order) <u>U</u>niform load, <u>R</u>ight-<u>H</u>alf load for the two- and three-material cases, and the <u>B</u>arry-<u>M</u>ercer problem. The three-material case is used when $\bar{p}_s$ is present, otherwise the two-material case is used.

(a) Triangular elements

u	$\bar{p}_s$	v_D	p_f	U	RH	BM
P_1	—	—	P_1	fail	fail	fail
P_2	—	—	P_2	fail	fail	fail
P_1^+	—	—	P_1	OK*	OK*	OK*
P_2	—	—	P_1	OK*	OK*	OK*
P_2	—	RT$_1$	P_0	OK	OK	OK
CR$_1$	—	RT$_1$	P_0	fail†	fail†	fail†
P_2	—	P_2	P_1	OK*	OK*	OK*
P_2^+	—	P_2^+	P_{-1}	OK	OK	OK
P_1^+	P_1	—	P_1	OK*	OK*	OK
P_1^+	P_1	RT$_1$	P_0	fail	fail	fail
P_2^+	P_{-1}	RT$_1$	P_0	OK	OK	OK
P_2	P_0	RT$_1$	P_0	OK	OK	OK
P_2^+	P_{-1}	P_2^+	P_{-1}	OK	OK	OK

(b) Quadrilateral elements

u	$\bar{p}_s$	v_D	p_f	U	RH	BM
Q_1	—	—	Q_1	fail	fail	fail
Q_2	—	—	Q_2	fail	fail	fail
Q_1^{++}	—	—	Q_1	OK*	OK*	OK*
Q_2	—	—	Q_1	OK*	OK*	OK*
Q_2	—	RT$_1$	Q_0	OK	OK	OK
TR$_1$	—	RT$_1$	Q_0	fail‡	fail‡	OK
Q_1	—	RT$_1$	Q_0	OK	OK	fail
Q_2	—	Q_2	Q_0	OK	OK	OK
Q_1^{++}	Q_1	—	Q_1	OK*	OK*	OK
Q_2	P_{-1}	—	Q_1	OK*	OK*	OK*
TR$_1$	Q_0	RT$_1$	Q_0	OK	fail	OK
Q_1	Q_0	RT$_1$	Q_0	OK	OK	fail
Q_2	P_{-1}	Q_2	P_{-1}	OK	OK	OK

*Continuous pressure elements exhibit local pressure spikes
†Singular coefficient matrix
‡Succeeds when tangential displacement BCs are added

compressive force of unit magnitude is instantaneously applied. In this case, both continuous and discontinuous elements lead to some overshoot of the fluid pressure, as shown in Figure 8c. In contrast to the earlier case, this problem cannot be well approximated with a small number of elements; arguably, the best approximation to the continous pressure solution at early times is a constant ($p_f = 1$), but this solution violates the essential boundary condition at the drained end ($p_f = 0$). Hence, this problem requires additional stabilisation to avoid initial oscillations for short time steps [7, 8, 9].

Depending on the model and on the desired properties of the solution, we list some combinations of element spaces that we find attractive.

- For a fast solver, the two-field formulation may be desirable. The fluid pressure solution must then be a subspace of H^1, (i.e., continuous), and localised pressure oscillations are unavoidable, as remarked above, unless stabilisation is added (such as the flow perturbation proposed by Aguilar *et al.* [7]). The MINI element combination (P_1^+/P_1), or its quadrilateral analogue (Q_1^{++}/Q_1) are attractive choices. The Taylor-Hood element (P_2/P_1 or Q_2/Q_1) is also stable, but the higher accuracy in u may be wasted since v_D is only piecewise constant.
- If higher accuracy of v_D is required, the fluid velocity three-field solution is warranted. A popular choice for the fluid velocity is the lowest order Raviart-Thomas elements, with piecewise constant fluid pressure. However, the simplest Stokes-stable element to combine with piecewise constant pressure is Crouzeix-Raviart (or Rannacher-Turek for quadrilaterals), which we found to be problematic. One would then have to use quadratic displacement ($P_2/$RT$_1 P_0$ or $Q_2/$TR$_1 Q_0$), which is rather expensive for a method which is still only first order accurate in the velocity. An

Copyright © 2000 John Wiley & Sons, Ltd.
Prepared using nagauth.cls

Int. J. Numer. Anal. Meth. Geomech. 2000; **0**:0–0

(a) Three-layer problem using Q_2/Q_1 and $\epsilon = 10^{-8}$

(b) Three-layer problem; Q_2/Q_2P_{-1} and $\epsilon = 10^{-8}$

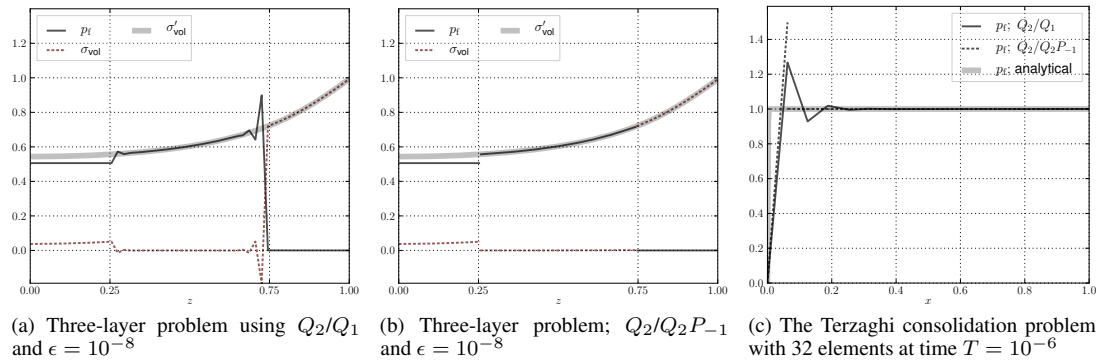(c) The Terzaghi consolidation problem with 32 elements at time $T = 10^{-6}$

Figure 8: Using discontinuous elements for the fluid pressure (b) avoids local oscillation at the edge of the low-permeable material, where the pressure gradient is very steep. It does not, however, smoothly handle the pressure front in early stages of the Terzaghi consolidation problem (c).

  alternative might be to follow the precept of Phillips and Wheeler [10], and use the Discontinuous Galerkin method for the displacement, or to use a variant which has second order accuracy also for the velocity (such as $P_2^+/P_2^+ P_{-1}$ or Q_2/Q_2P_{-1}).

- When low-compressible materials are present, the solid pressure three-field formulation (or even the four-field formulation) may be required. A good choice for the former appears to be the MINI combination $P_1^+ P_1/P_1$ or $Q_1^{++} Q_1/Q_1$, although the problem of localised oscillations in both fluid and solid pressure around discontinuities reappears. For the four-field formulation, we recommend $P_2^+ P_{-1}/P_2^+ P_{-1}$ or the quadrilateral $Q_2 P_{-1}/Q_2 P_{-1}$.

6. Concluding remarks

In this paper we have investigated the spurious pressure oscillations that are present in the finite element solution of the poroelastic equations for small time steps and low-permeable materials.

Through comparison with the displacement-solid pressure mixed formulation of linear elasticity, we identify the spurious pressure modes as a specific consequence of a vanishing Brezzi inf-sup constant β_h. Since the Brezzi inf-sup condition for the poroelastic equations takes on a similar form as in, e.g., the mixed linear elasticity or Stokes problem, this identification opens up the field to a plethora of stable element candidates. These can be used directly for the basic solid displacement-fluid pressure two-field formulation of poroelasticity, or in combinations for the various three- and four-field formulations involving solid pressure and/or fluid velocity.

Extensive numerical investigation of the stability of a large set of two-, three- and four-field models have been performed. These investigations provide evidence that most of the element combinations recommended by our theoretical guidelines give oscillation-free solutions for the pressure.

The authors would like to thank Dr. Marie Rognes at Simula Research Laboratory for her contributions to the present paper.

References

[1] Biot MA. General theory of three-dimensional consolidation. *Journal of Applied Physics* 1941; **12**(2):155–164, doi:10.1063/1.1712886.

[2] Vermeer PA, Verruijt A. An accuracy condition for consolidation by finite elements. *International Journal for Numerical and Analytical Methods in Geomechanics* 1981; **5**(1):1–14, doi:10.1002/nag.1610050103.

[3] Zienkiewicz O, Chan A, Pastor M, Paul D, Shiomi T. Static and dynamic behaviour of soils: a rational approach to quantitative solutions. I. fully saturated problems. *Proceedings of the Royal Society of London. Series A, Mathematical and Physical Sciences* 1990; **429**(1877):285–309.

[4] Murad MA, Loula AFD. On stability and convergence of finite element approximations of Biot's consolidation problem. *International Journal of Numerical Methods in Engineering* 1994; **37**:645–667, doi:10.1002/nme.1620370407.

[5] Murad MA, Thomée V, Loula AFD. Asymptotic behavior of semidiscrete finite-element approximations of Biot's consolidation problem. *SIAM Journal on Numerical Analysis* 1996; **33**(3):1065–1083, doi:10.1137/0733052.

[6] Wan J. Stabilized finite element methods for coupled geomechanics and multiphase flow. PhD Thesis, Stanford University 2003.

[7] Aguilar G, Gaspar F, Lisbona F, Rodrigo C. Numerical stabilization of Biot's consolidation model by a perturbation on the flow equation. *International Journal of Numerical Methods in Engineering* 2008; **75**(11):1282–1300, doi:10.1002/nme.2295.

[8] Korsawe J, Starke G. A least-squares mixed finite element method for Biot's consolidation problem in porous media. *SIAM Journal on Numerical Analysis* 2006; **43**(1):318–339, doi:10.1137/S0036142903432929.

[9] Tchonkova M, Peters J, Sture S. A new mixed finite element method for poro-elasticity. *International Journal for Numerical and Analytical Methods in Geomechanics* 2008; **32**(6):579–606, doi:10.1002/nag.630.

[10] Phillips P, Wheeler M. A coupling of mixed and discontinuous Galerkin finite-element methods for poroelasticity. *Computational Geosciences* 2008; **12**(4):417–435, doi:10.1007/s10596-008-9082-1.

[11] Bathe KJ. *Finite Element Procedures*. Prentice Hall, 1996.

[12] Dean RH, Gai X, Stone CM, Minkoff SE. A comparison of techniques for coupling porous flow and geomechanics. *SPE Journal* Mar 2006; **11**(1):132–140, doi:10.2118/79709-PA.

[13] Phillips PJ, Wheeler MF. Overcoming the problem of locking in linear elasticity and poroelasticity: an heuristic approach. *Computational Geosciences* 2009; **13**(1):5–12, doi:10.1007/s10596-008-9114-x.

[14] Liu R, Wheeler MF, Dawson CN. Discontinuous Galerkin finite element solution for poromechanics. PhD Thesis, University of Texas at Austin 2006.

[15] Barry SI, Mercer GN. Flow and deformation in poroelasticity—I unusual exact solutions. *Mathematical and Computer Modelling* 1999; **30**(9):23–29, doi:10.1016/S0895-7177(99)00177-6.

[16] Neuzil CE. Hydromechanical coupling in geologic processes. *Hydrogeology Journal* 2003; :11:41–83.

[17] Brezzi F. On the existence, uniqueness and approximation of saddle-point proble arising from Lagrangian multipliers. *RAIRO Analyse Numérique* 1974; **R–2**:129–151.

[18] Babuška I. The finite element method with Lagrangian multipliers. *Numerische Mathematik* 1973; **20**(3):179–192, doi:10.1007/BF01436561.

[19] Chapelle D, Bathe KJ. The inf-sup test. *Computers & Structures* 1993; **47**(4–5):537–545, doi:10.1016/0045-7949(93)90340-J.

[20] Qin J. On the convergence of some low order mixed finite elements for incompressible fluids. PhD Thesis, The Pennsylvania State University 1994.

[21] Rognes ME. Automated testing of saddle point stability conditions. Unpublished, to appear in Logg A, Mardal KA, Wells GN (eds.) *Automated Scientific Computing.* Springer.

[22] Gresho PM, Sani RL. *Incompressible Flow and the Finite Element Method. Volume 2: Isothermal Laminar Flow*. John Wiley and sons, 1998.

[23] Crouzeix M, Raviart PA. Conforming and nonconforming finite element methods for solving the stationary Stokes equations. *RAIRO Analyse Numérique* 1973; **7**:33–75.

[24] Arnold DN, Brezzi F, Fortin M. A stable finite element for the Stokes equations. *Calcolo* 1984; **21**(4):337–344, doi:10.1007/BF02576171.

[25] Bai W. The quadrilateral 'Mini' finite element for the Stokes problem. *Computer Methods in Applied Mechanics and Engineering* 1997; **143**:41–47, doi:10.1016/S0045-7825(96)01146-2.

[26] Wang HF. *Theory of Linear Poroelasticity with Applications to Geomechanics and Hydrogeology*. Princeton University Press, 2000.

Copyright © 2000 John Wiley & Sons, Ltd.
Prepared using nagauth.cls

Int. J. Numer. Anal. Meth. Geomech. 2000; **0**:0–0